

3. Normal State

3.1 Time integration

As already indicated in section 2.7, the calculation was carried out in two stages. The integration of stage I, in which $\Delta\lambda=5.0^\circ$, was made over a period of 100 years, starting from the initial state given in section 2.6. Then, instantaneous fields at the end of stage I were interpolated linearly to the grids of stage II, in which $\Delta\lambda=2.5^\circ$, and the stage II was calculated for another 40 years.

Fig. 3-1(a) shows the time history of the overall mean kinetic energies. The total kinetic energy reaches its maximum value at the beginning of each stage, the 220th day of stage I and the 60th day of stage II. Then, it begins to decrease until the 6th year of stage I and the 220th day of stage II. For the rest of each stage, the total kinetic energy

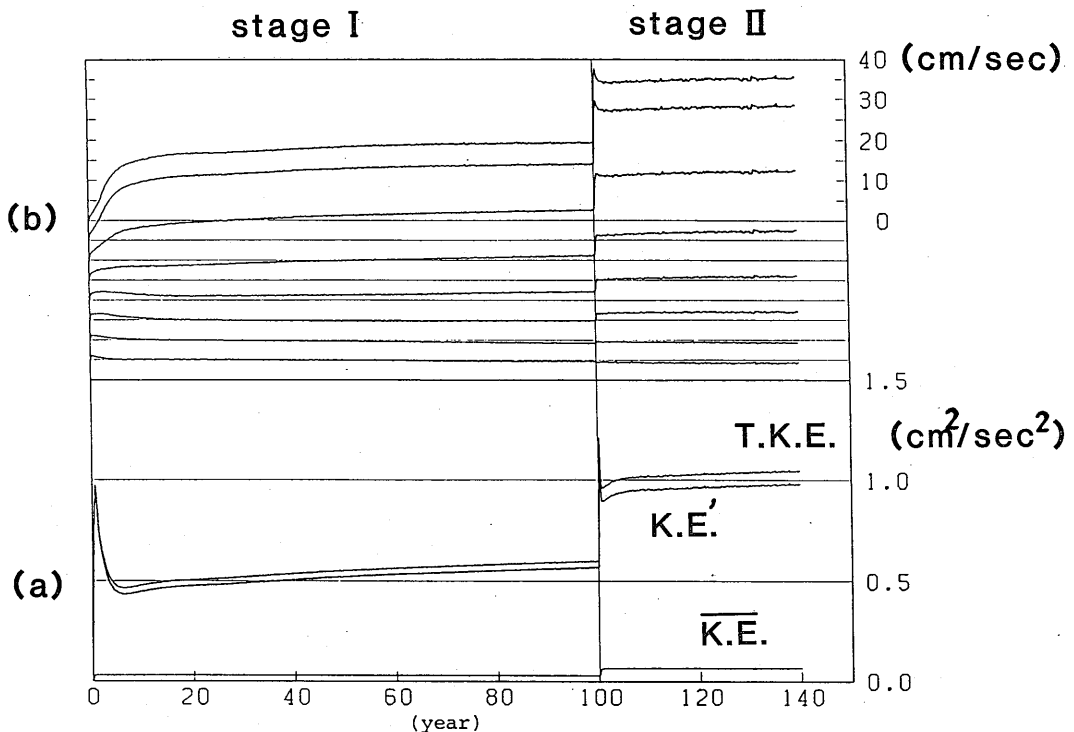


Fig. 3-1 (a) Time history of the overall mean kinetic energies per unit mass. $\overline{K.E.}$, $K.E.'$, and $T.K.E.$ mean the kinetic energies of the vertical mean current, vertical shear current, and total current, respectively.

(b) Time development of the western boundary current at $(33^\circ\text{N}, 2.5^\circ\text{E})$ during stage I and at $(33^\circ\text{N}, 1.25^\circ\text{E})$ during stage II. The curves correspond to the northward velocities at level 1 (top) through level 8 (bottom).

continues to increase very slowly. Almost 95% of the kinetic energy is contributed by the vertical shear current. The kinetic energy of the vertical mean current is almost constant except for the first 100 days of each stage. (It should be remembered that the rate of change of the vertical mean current was reduced to one tenth in the present model.) The available potential energy (not shown here) increases from zero at the initial time to $415(\text{cm}/\text{sec})^2$ at the end of the 140th year. The northward component of the western boundary current is shown as a function of time in Fig. 3-1(b). The current continues to speed up in the upper ocean except for a short term at the beginning of stage II.

The thermal response is rapid near the surface, and the temperature averaged over level 1 is almost constant during the last 60 years. On the other hand, the mean temperatures of levels 5 and 6 increase at the rate of $0.01\sim 0.02^\circ\text{C}/\text{year}$ in stage II. This reflects that the thermocline given as an initial state diffuses with time. The overall mean temperature continues to increase slowly throughout the computation. An inspection of the time development of the temperature and salinity patterns in a meridional plane along the central longitude shows that their main features are developed during the first 50 years.

In this chapter the final state of stage II, which is defined as the normal state in the subsequent studies, is described briefly. Overall characteristics are similar to the numerical solutions of Bryan and Cox (1968), Haney (1974), and Takano (1981).

3.2 Horizontal distributions

Fig. 3-2 shows the stream function of the vertically integrated transport. Five circulation gyres are developed in the model ocean. The general characteristics of the pattern, such as the latitudinal extent, relative strength, and rotating direction of each gyre, are basically identical to those predicted by the Stommel-Munk theory of a wind-driven ocean. But there are some discrepancies. The maximum poleward transport, for example, by the anticyclonic subtropical gyre in the northern ocean occurs at 28°N , while the wind stress curl is maximum at 30°N . The maximum transport of $44.8 \times 10^{12} \text{ cm}^3/\text{sec}$ is smaller by about 20% than that computed according to the Sverdrup relation, 55.4×10^{12} . These discrepancies are mainly caused by the smoothing effect of the large eddy viscosity used in the model. In fact, the transport given by the Sverdrup relation is 29.8×10^{12} at 26°N , 36.2×10^{12} at 28°N , 38.4×10^{12} at 32°N , and 12.8×10^{12} at 34°N (cf. Fig. 3-13, which shows a result for a weakly viscous model).

The fields of temperature, salinity, density, and horizontal velocity at level 1 are shown

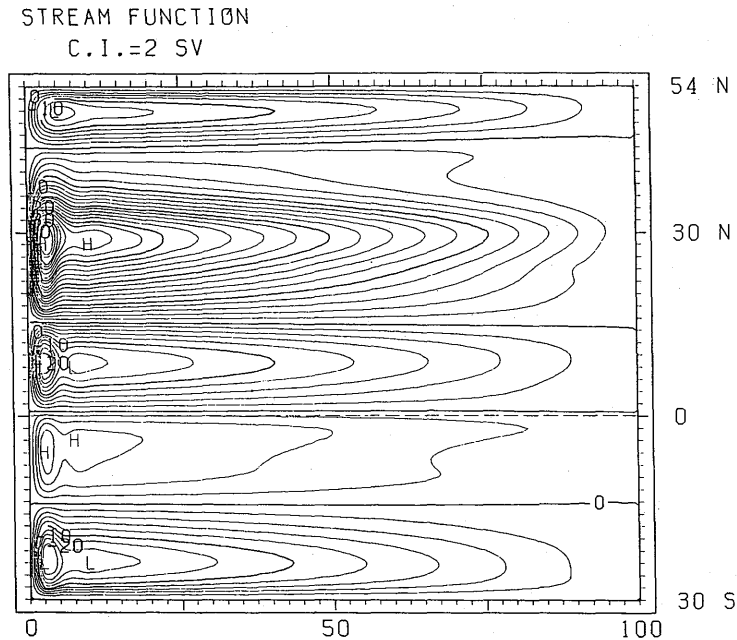


Fig. 3-2 Stream function of the vertically integrated transport. The contour interval is given at the top left. Thick lines are drawn every five intervals. $1 \text{ SV} = 10^6 \text{ m}^3/\text{sec}$.

in Figs. 3-3(a) through (d). Although the general patterns of isotherms and isohalines are zonal and are principally governed by the external parameters T_a^* and $(P-E)$, several features dynamically produced are clearly seen. In particular, a cold water band is developed along the equator where T_a^* is maximum. This is a result of the strong divergence of the wind-driven Ekman currents, which builds up a narrow band of strong upwelling (w is 5×10^{-3} cm/sec at the bottom of the uppermost layer) along the equator. In addition, there is a warm tongue extending northward along the western boundary in the north subtropical latitudes. This feature is due to the horizontal temperature advection in the anticyclonic gyre. The model analog of the subtropical front can be seen in the temperature field between 25°N and 30°N , which shifts northward in the eastern part of the ocean (Takeuchi, 1984).

The density distribution is primarily determined by the temperature. The salinity acts to strengthen the density front around 20°N , and to weaken it north of about 25°N .

The current vectors clearly show the model analogs of the Kuroshio, the North Pacific Current, and the Subtropical Counter Current. The western boundary current attains a

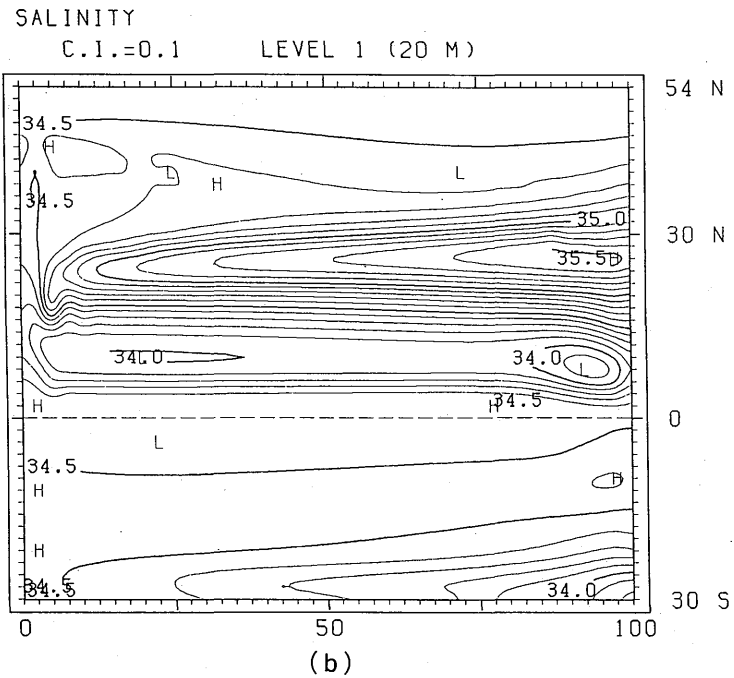
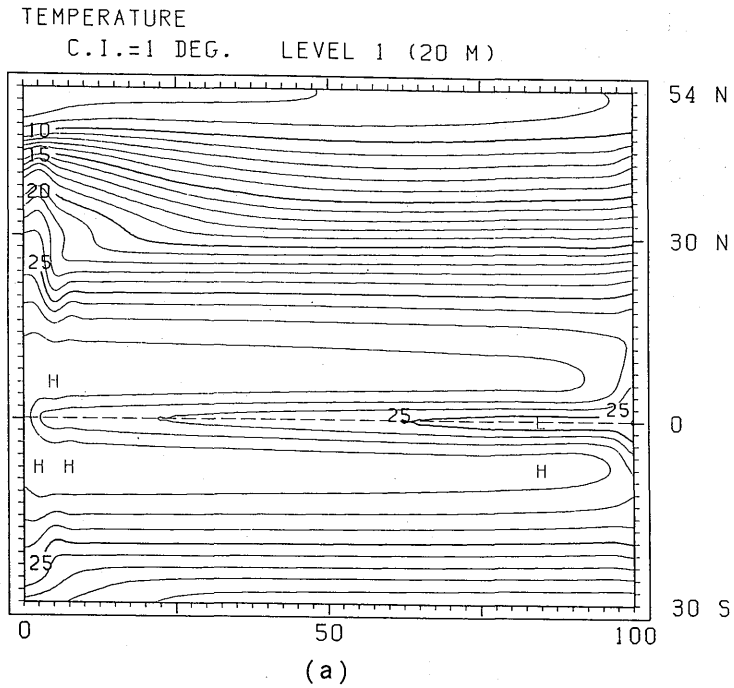
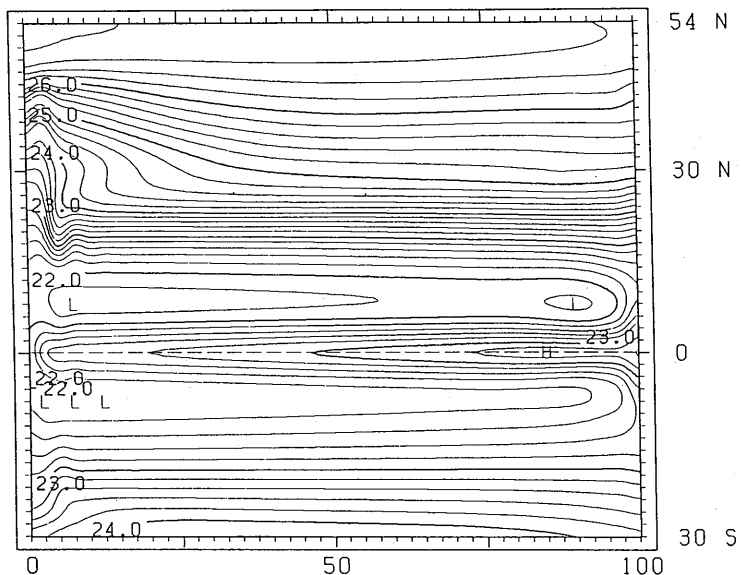


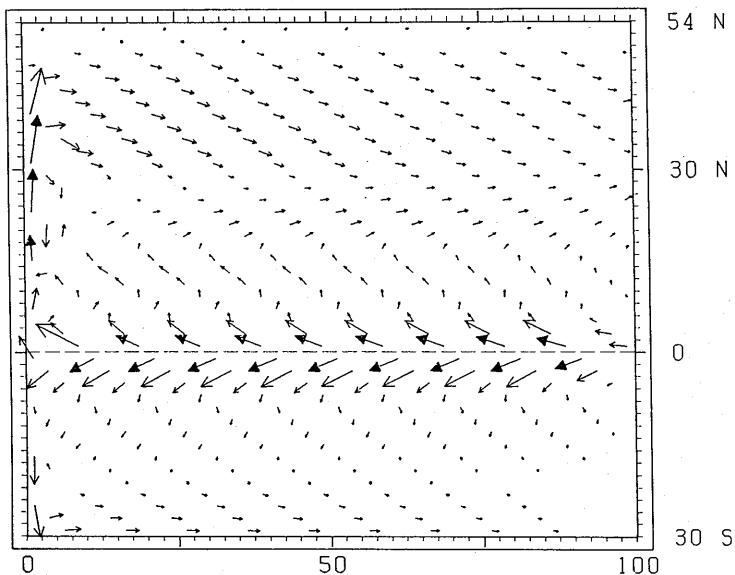
Fig. 3-3 (a) Temperature, (b) salinity, (c) density, and (d) horizontal velocity vectors at level 1. Velocity vectors are plotted only at every 10° of longitude. The arrows are scaled by the vectors given at the top left.

DENSITY IN SIGMA T
C.I.=0.2 LEVEL 1 (20 M)



(c)

HORIZONTAL VELOCITY
→ : 10 → : 20 CM/S LEVEL 1 (20 M)



(d)

Fig. 3-3 Continued.

maximum speed of 40 cm/sec at 31°N. The model analogs of the North Equatorial Counter Current and the North Equatorial Current, on the other hand, are very weak. In the tropical latitudes the currents have a discernible poleward component, of which the dominant part is the Ekman current driven by the easterly wind stress. As a result the zonality of currents in the tropics is very poorly reproduced. The analogs of the California Current and westward subarctic currents are completely missing at level 1.

Figs. 3-4(a) and (b) show the temperature and velocity fields at level 2. The cold water along the equator is much less extensive than at level 1, and a warm water pool is developed in the western part of the tropics. The flow pattern near the equator is a reversal of that at level 1. The model analog of the Equatorial Undercurrent is produced, though it has a considerable equatorward component. (It should be noted that velocity vectors are plotted at every fourth grid in the longitudinal direction.) The subsurface extension of the model's North Equatorial Counter Current at 7°N is merged with the equatorial undercurrent. The subtropical gyre of the northern ocean is clearly seen at level 2 since the model's North Equatorial Current is stronger than at level 1. But the eastward transport in the gyre is much larger than the westward transport. A large part of the eastward flowing mass bumps against the eastern boundary and sinks to deeper layers there. Weak westward currents are seen along the northern boundary. The model's Equatorial Undercurrent is almost zonal at level 3 (not shown here).

Figs. 3-5(a) and (b) show the temperature and velocity fields at level 4. The temperature is relatively low in the tropical region, and warm water pools are developed in the subtropics. In the equatorial region, noted are the eastward currents symmetrically located about the equator. In the eastern half of the equator, they are separated by westward currents centered on the equator. The eastward currents are the model analog of the Equatorial Subsurface Counter Currents. The most unrealistic feature of level 4 is a warm tongue extending west-southwestward from the eastern boundary near 30°N. The warm water is supplied by strong downwellings in the vicinity of the eastern boundary, and it is advected along the southern flank of the subtropical gyre. (The realistic temperature pattern is a westward intensified pool of warm water, like that produced in the southern ocean.) The same unrealistic feature is also seen at level 3, where a warm tongue is generated around 25°N.

The fields at the lower four levels are not shown here. The warm tongue extending from the eastern boundary is also seen at level 5 and level 6 around 38°N and 44°N, re-

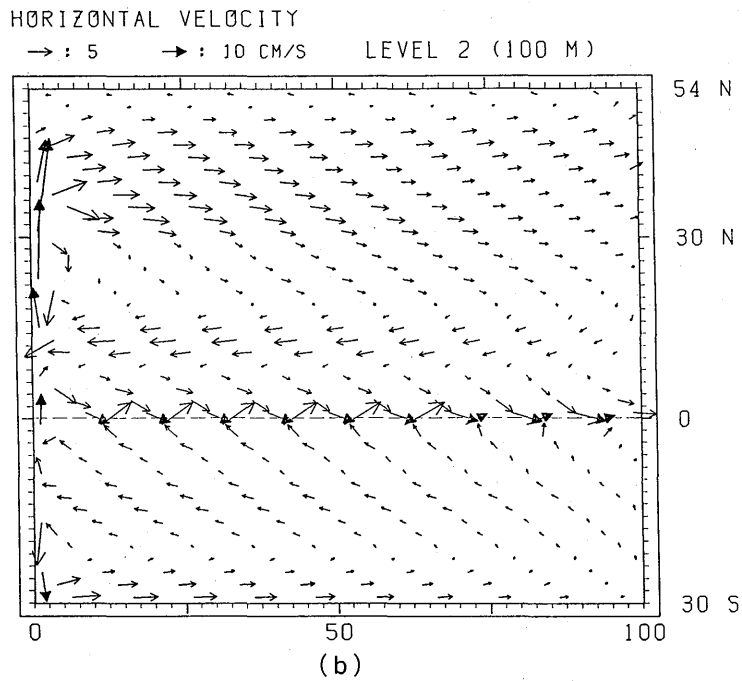
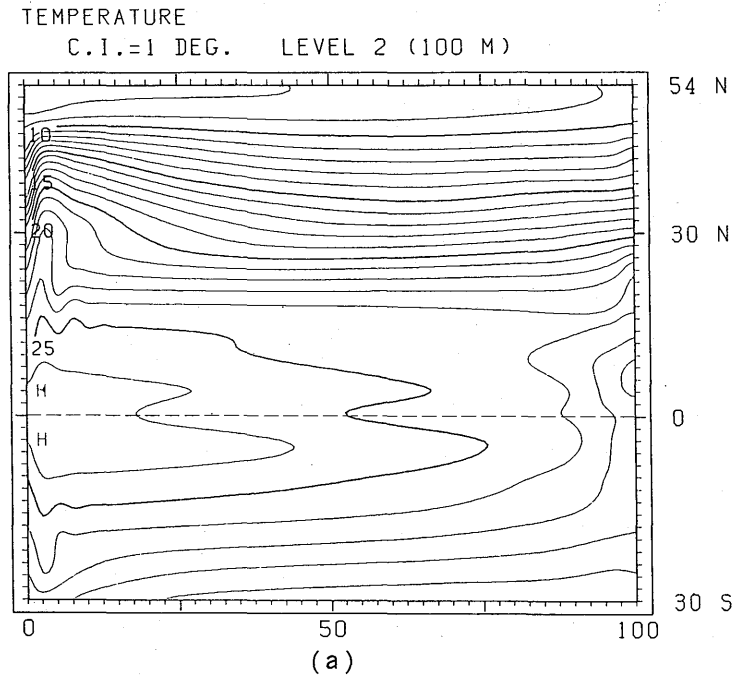
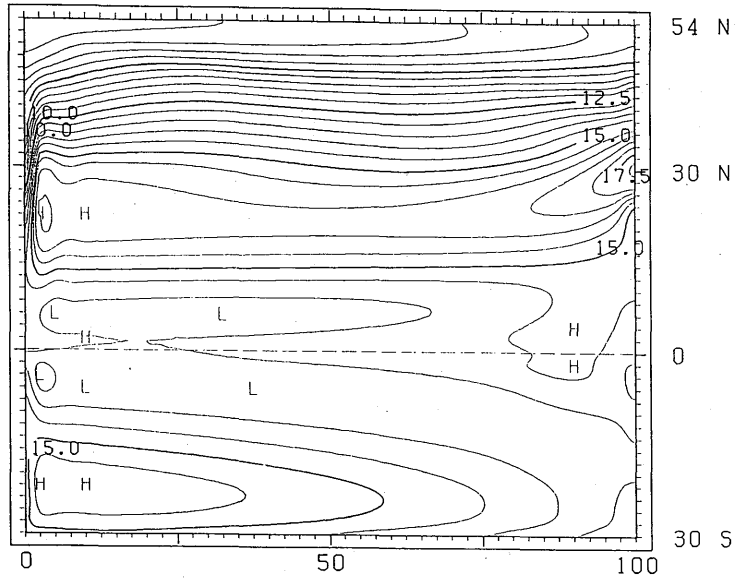


Fig. 3-4 (a) Temperature and (b) horizontal velocity vectors at level 2.

TEMPERATURE

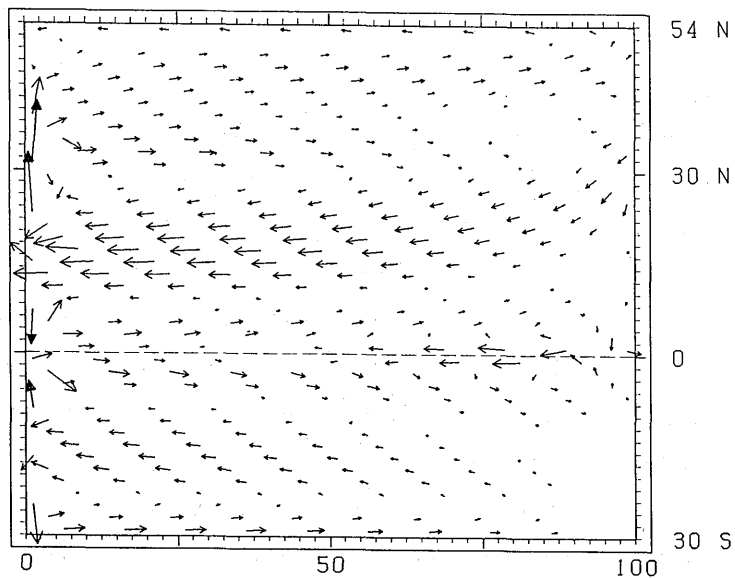
C.I.=0.5 DEG. LEVEL 4 (480 M)



(a)

HORIZONTAL VELOCITY

→ : 3 → : 6 CM/S LEVEL 4 (480 M)



(b)

Fig. 3-5 As in Fig. 3-4 except for level 4.

spectively. At level 7 warm temperatures are produced in the vicinity of the northern boundary.

3.3 Vertical sections

The three-dimensional structure of physical property is almost uniform in the zonal direction except near the western and eastern boundaries. Figs. 3-6(a), (b), and (c) show the distribution of temperature, salinity, and density in a cross-section along the central longitude. (Note that in the following vertical sections, the uppermost one kilometer of the ocean is shown in an expanded scale.) The temperature section shows a tendency for the thermocline to be shallow in the equatorial region. Near 8°N the thermocline bifurcates into an upper and a lower portion. The upper one gradually shallows poleward and surfaces at about 25°N. It is associated with the model's Subtropical Counter Current. The lower one, which slopes down toward the north, is associated with the westward flowing branch of the subtropical gyre. The water below 1 km has no outcrop at the surface, since the convective overturning adjacent to the northern boundary penetrates only to 1 km. (In the vicinity of the eastern boundary the convective overturning penetrates down to about 2 km. See Fig. 3-8 (a).)

In the salinity section, relatively high or low salinity water is extended downward from the sea surface with the latitude where the imposed ($P-E$) takes a minimum or maximum value.

The salinity-minimum layer at an intermediate depth extending southward from the subarctic, which is one of the most salient features observed in the North Pacific, is not reproduced. The density field is quite similar to that of temperature.

Fig. 3-6(d) shows a cross-section of the eastward velocity component. The vertical profile is complicated at the equator where eastward and westward currents alternate between level 5 and level 8. The eastward velocity corresponding to the model's North Equatorial Counter Current is only slightly discerned and merges with the model's Equatorial Undercurrent as described above.

In the northern extratropics there are three maxima of eastward current speed. One at 23°N corresponds to the model's Subtropical Counter Current. The other two are caused by the latitudinal profile of the imposed wind stress curl (cf. Fig. 3-12).

The temperature section along the equator is shown in Fig. 3-7. The model reproduces two interesting features which are also seen in the observed temperature sections (Moore and

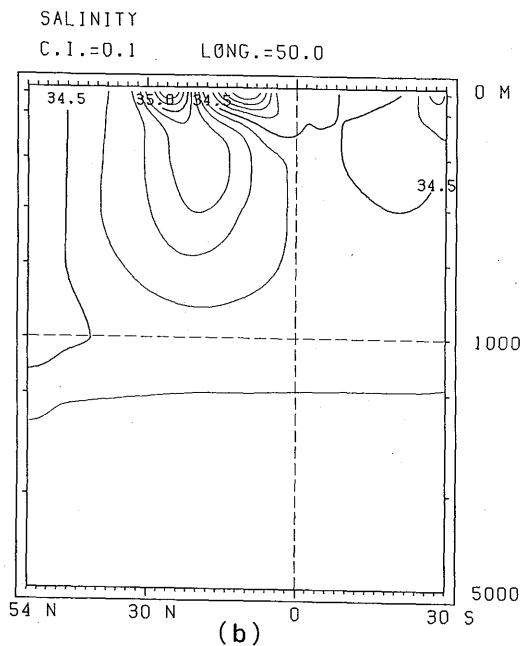
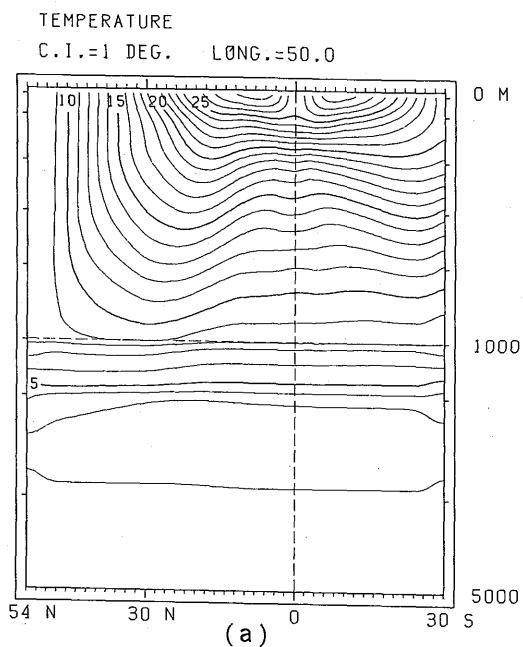


Fig. 3-6 Vertical sections of (a) the temperature, (b) salinity, (c) density, and (d) zonal velocity component. (a), (b), and (c) are along 50°E, and (d) is along 51.25°E. Westward motion is shaded. The vertical scale is exaggerated in the upper one kilometer.

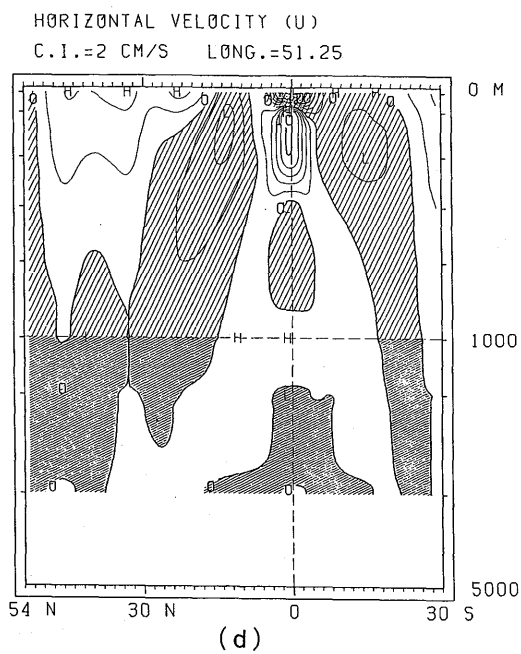
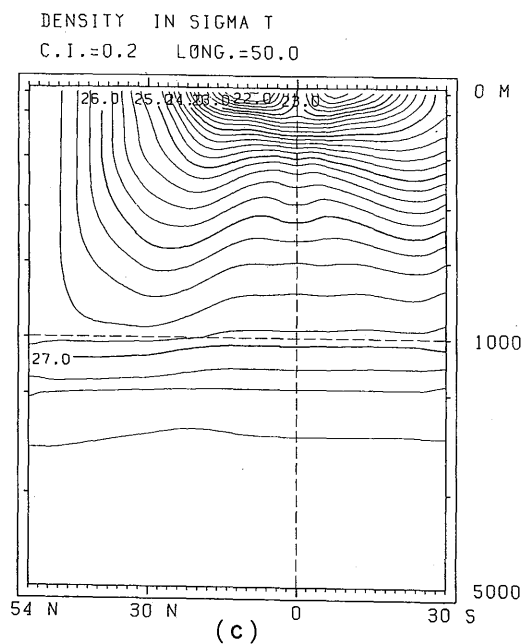


Fig. 3-6 Continued.

TEMPERATURE

C.I.=1 DEG. LAT.=0

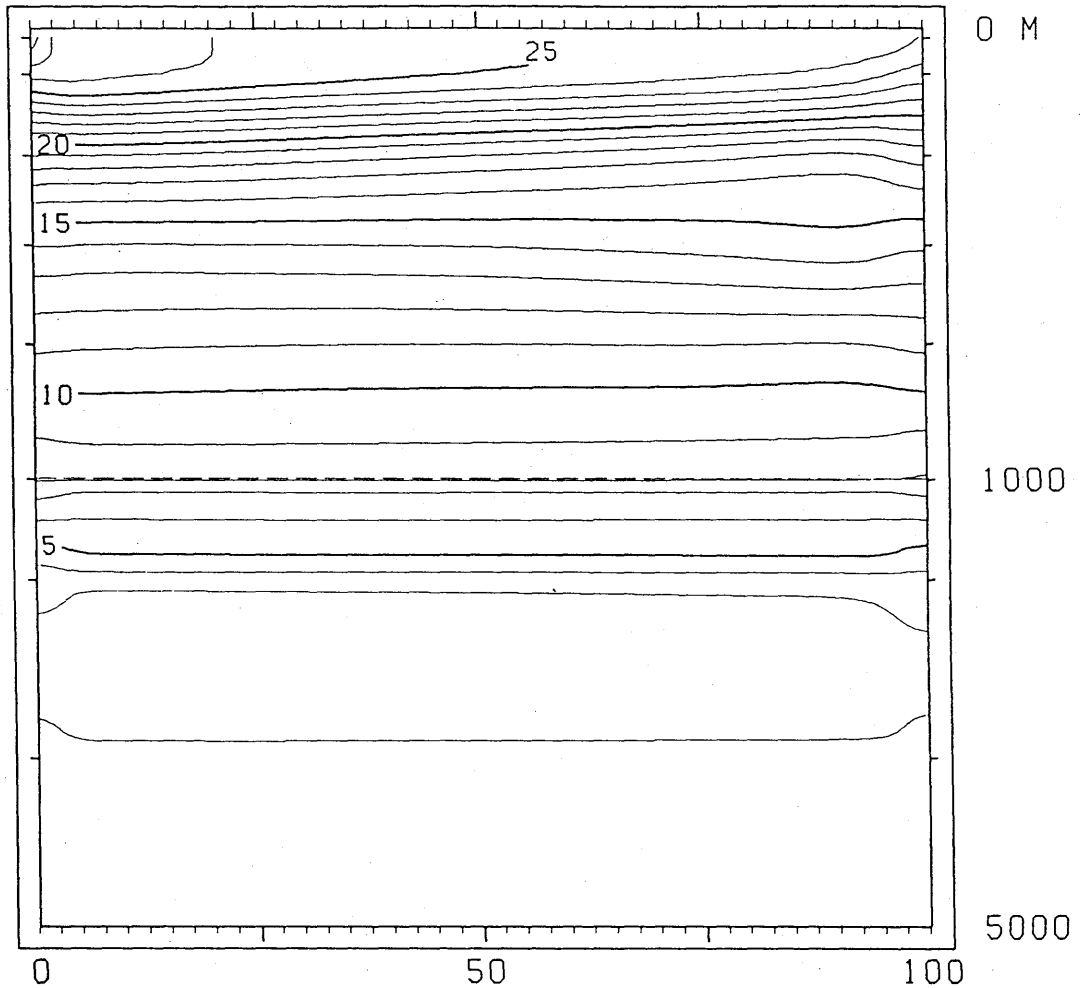


Fig. 3-7 A vertical section of the temperature along the equator.

Philander, 1977). The first is the thermocline which slopes upward to the east. The second is a relatively homogeneous layer near 400 m in the eastern equatorial region. (The model's Equatorial Subsurface Counter Currents described in the preceding section are located at the poleward ends of this thermostat.) The degree of similarity, however, is not satisfactory. The thermocline in the observed sections is sharper and shallower in the eastern region. Furthermore, the thermostat is located at a shallower depth of 200–300 m. It is also noted that the model does not produce the correct zonal gradient of surface temperature. In

observations, the zonal temperature gradient is large in the eastern region and relatively isothermal warm water is located in the western region. In the model, on the other hand, the gradient is relatively large near the western boundary (see Fig. 3-3(a)). This discrepancy can be partly attributed to the zonal structure of the wind stress. A zonally uniform stress is imposed in the model, while several analyses of the tropical wind field (Wyrtki and Meyers, 1976) indicate that the annual mean wind stress significantly varies in the zonal direction and the westward wind is strongest in the central Pacific Ocean.

Now the vertical thermal structure associated with the warm tongue seen in the southern flank of the northern subtropical gyre is described. Fig. 3-8(a) shows the vertical temperature section along the eastern boundary. It indicates that, north of 20°N, surface warm water penetrates to a greater depth with latitude. The zonal temperature section along 30°N, which cuts through the center of the subtropical gyre, is shown in Fig. 3-8(b). The isotherm pattern is not realistic in the eastern part where strong downwelling takes place. In observed sections, isotherms generally slope upward to the east except in the western boundary current region.

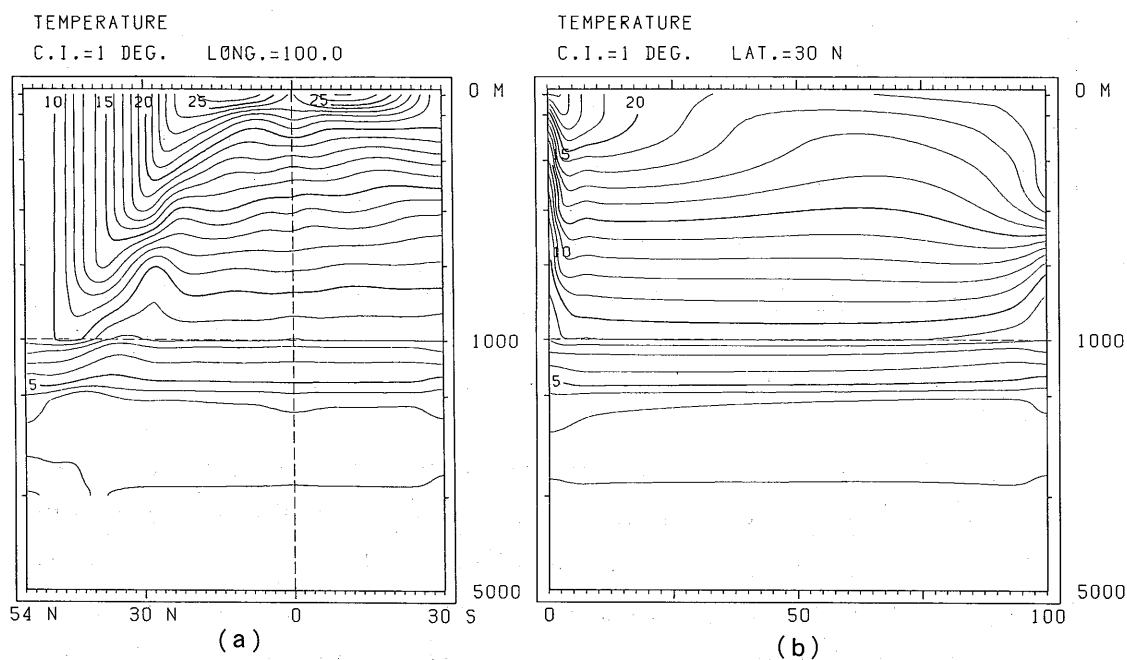


Fig. 3-8 Vertical sections of the temperature along (a) the eastern boundary (100°E) and (b) 30°N.

3.4 Meridional circulation and meridional heat transport

Integrating the continuity equation (2-5) from the western to the eastern boundary, the following equation is obtained:

$$\int_0^{100\pi/180} \cos\phi \frac{\partial w}{\partial z} d\lambda + \int_0^{100\pi/180} \frac{\partial}{\partial \phi} (v \cos\phi) d\lambda = 0. \quad (3-1)$$

From this relationship the meridional circulation integrated over the zonal extent of the ocean basin can be specified in terms of a transport stream function Φ , such that

$$\int_0^{100\pi/180} a \cos\phi \cdot w d\lambda = \frac{\partial \Phi}{\partial \phi},$$

$$\int_0^{100\pi/180} a \cos\phi \cdot v d\lambda = -\frac{\partial \Phi}{\partial z}. \quad (3-2)$$

The streamfunction is shown in Fig. 3-9. A direct meridional cell of basin-wide scale dominates in the northern ocean. The general sinking motion, which primarily occurs near the eastern boundary, extends deep to the north. This thermohaline circulation is confined to the upper 2 km, and the abyssal part of the basin is isolated. The isolated water, whose temperature and salinity gradually change from each initial value mainly due to vertical diffusion, is heavier than the dense water formed by the model cooling. The shallow cells in the equatorial region are primarily wind-driven.

Fig. 3-10 shows the heat flux through the ocean surface. Major heating occurs in the equatorial region, and major cooling occurs in the western boundary region of the northern subtropics and in the northern boundary region. Weak cooling and heating occur in the northern interior region between 13°N and 25°N and between 25°N and 40°N, respectively. In an equilibrium state, the heat absorbed in the tropics must be transported poleward to compensate the upward heat flux in the higher latitudes. The total meridional heat transport is given by

$$H = \rho_0 c_p \int_{-H}^0 \int_0^{100\pi/180} (vT - A_h \frac{\partial T}{\partial \phi}) a \cos\phi d\lambda dz$$

$$= \rho_0 c_p \int_{-H}^0 \int_0^{100\pi/180} (\bar{v}\bar{T} + \overline{v'T'}) - A_h \frac{\partial \bar{T}}{\partial \phi}) a \cos\phi d\lambda dz, \quad (3-3)$$

where the overbars indicate the zonal averages, and the primes the deviations from them. The first term represents the heat transport associated with the mean meridional circulation shown in Fig. 3-9. The second term is the effect of correlations between deviations from zonal averages, and represents the heat transport associated with horizontal gyres. The last

term represents the contribution of the northward diffusion of heat. The total heat transport and three components are shown in Fig. 3-11. The heat transport associated with the mean meridional circulation dominates except in the vicinity of the northern and southern boundaries where the effect of horizontal diffusion becomes significant. The total transport has a maximum value of $9 \times 10^{14} \text{W}$ at 15°N .

3.5 Comments

We describe here two aspects of the general circulation which the model fails to reproduce.

The first is on the North Equatorial Counter Current. The second is on the southward

MERIDIONAL CIRCULATION

C.I. = 2 SV

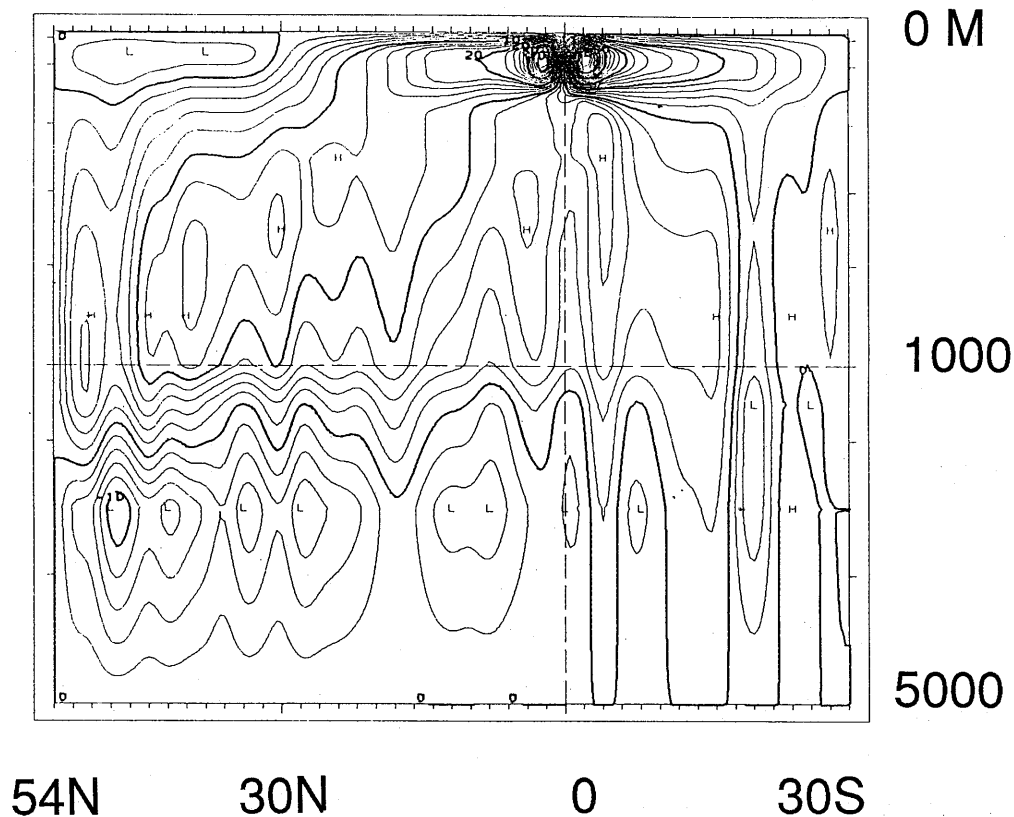


Fig. 3-9 Total transport in the meridional plane.

HEAT FLUX

C.I. = 10 W/M**2

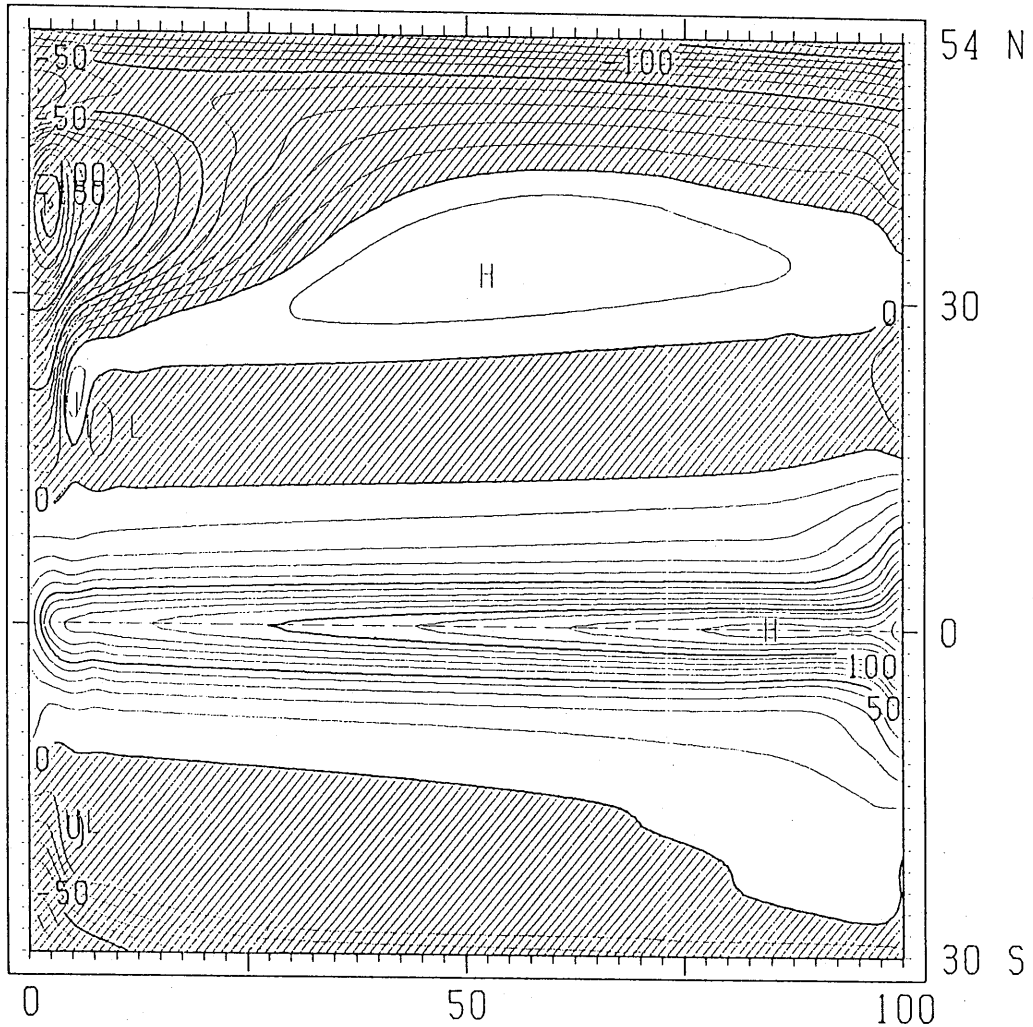


Fig. 3-10 Downward heat flux through the ocean surface.

currents in the eastern part of the northern subtropical gyre and the associated density structure. They are both one of the salient elements in the observed upper ocean structure.

Although these defects do not cause any significant errors in the response studies given in the next chapter, they would give quantitatively inaccurate results.

(1) In the tropics, currents are generally zonal and narrow in the north-south direction. It is supposed, therefore, that the lateral viscosity coefficient used in the model is too large

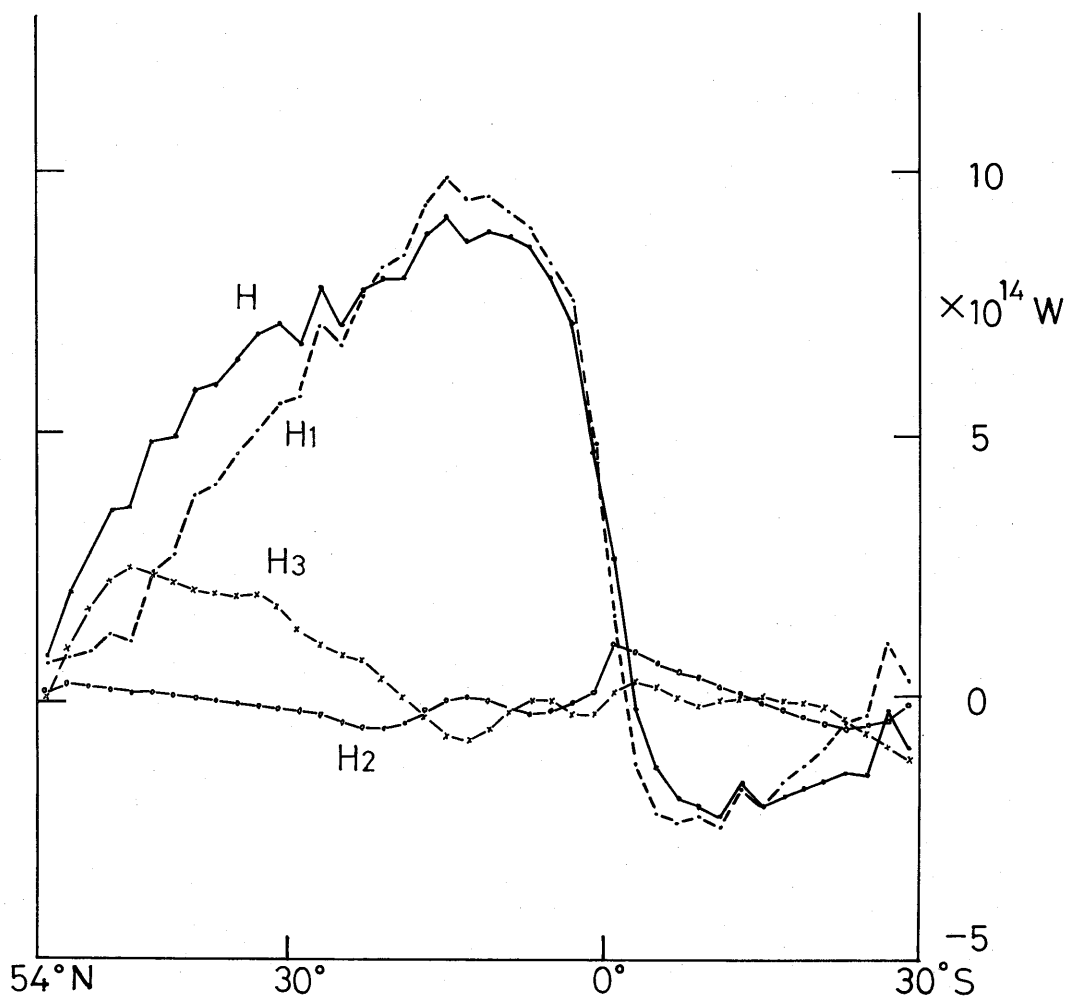


Fig. 3-11 Northward heat transport. H_1 , H_2 , H_3 , and H indicate the contributions of the mean meridional circulation, horizontal gyres, horizontal diffusion, and their sum, respectively.

to resolve the equatorial current pattern. From this viewpoint, a weakly viscous model, in which $A_m = 3.5 \times 10^7$ cm²/sec and $\Delta \lambda = 1.25^\circ$, was integrated over a period of 10 years, starting from the initial state of rest given in section 2.6. In this model, the salinity was held constant, i.e., $S = 34.5$, because salinity has only a minor effect on the density structure in the low latitudes.

Fig. 3-12 shows a meridional section of the eastward velocity component at the end of the 10th year. The model's North Equatorial Counter Current is clearly produced, with a core at the surface. It thus appears that the meridional grid distance of 2° would marginally

HORIZONTAL VELOCITY (U)

C.I. = 2 CM/S LONG. = 50.625

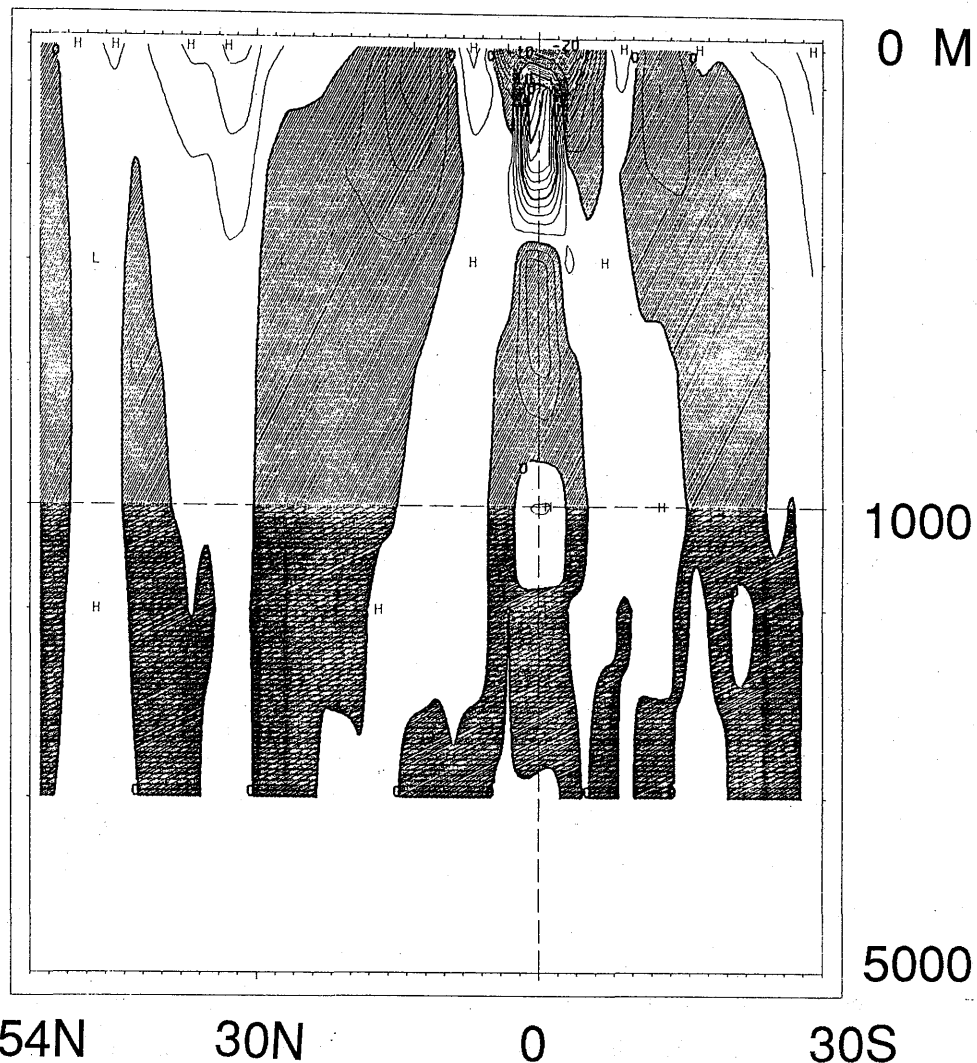


Fig. 3-12 As in Fig. 3-6 (d) except for the weakly viscous model and along 50.625°E.

resolve the equatorial current pattern if the viscosity coefficient is small enough. In the figure, an eastward cell, which is a south equatorial counter current, is also seen at 9°S. This is attributed to the imposed wind stress curl, having maxima at 2°S and 10°S. Fig. 3-13 shows the stream function of the vertically integrated transport. The southern tropical gyre and the northern subtropical gyre have both split into two gyres as a result of the reduction

STREAM FUNCTION

C.I. = 2 SV

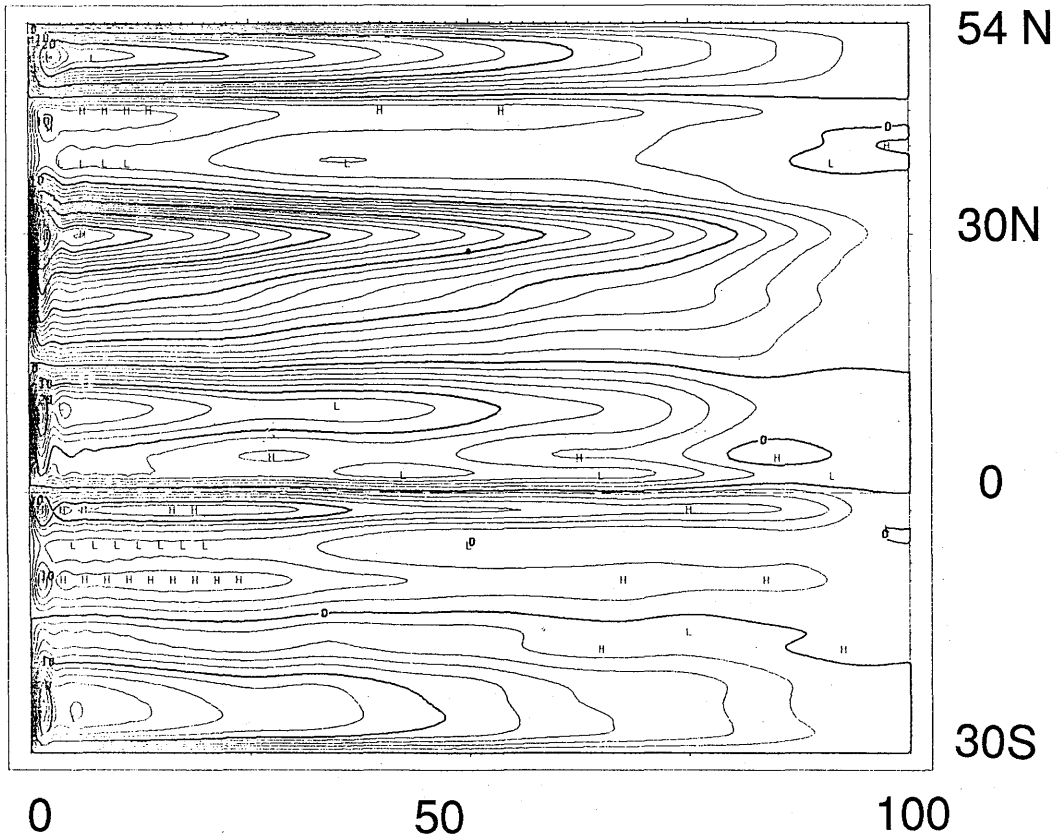


Fig. 3-13 As in Fig. 3-2 except for the weakly viscous model.

of viscosity (cf. Fig. 3-2). The split patterns reflect the curl τ pattern.

(2) In the eastern subtropics, the same feature, that is, a warm tongue extending westward from the eastern boundary, appears more or less in the results as previously reported, for example, by Haney (1974) and Takano (1981). (It is also seen in the result of an eddy resolving model by Han (1975), in which the calculation was started from the quasi-steady state obtained with a coarse grid model.)

This feature is due to the heat-driven circulation, as shown in Takano (1981). The upper boundary condition on temperature forces the temperature of the upper ocean to take a southward gradient in the eastern subtropics where horizontal currents are weak. Therefore, a baroclinic current normal to the boundary is developed near the eastern

boundary, where the vertical mean current has no normal component. (The warm tongue feature apparently does not appear in Semtner and Mintz (1977). The gradient of the apparent air temperature is not parallel to the eastern boundary in their model, but it is not clear how this condition affects the dynamics near the eastern boundary.)